Dynamics of $C_2H_2^{3+} \rightarrow H^+ + H^+ + C_2^+$ investigated by 50-keV/u Ne^{8+} impact

S. Xu,[1,*] X. L. Zhu,[2] W. T. Feng,[2] D. L. Guo,[2] Q. Zhao,[2,3] S. Yan,[2] P. Zhang,[2] D. M. Zhao,[2] Y. Gao,[2] S. F. Zhang,[2] J. Yang,[2] and X. Ma[2,†]

[1]*School of Science, Xi'an Jiaotong University, Xi'an 710049, China*

[2]*Institute of Modern Physics, Chinese Academy of Sciences, Lanzhou 730000, China*

[3]*School of Nuclear Science and Technology, Lanzhou University, Lanzhou 730000, China*

(Received 15 March 2018; published 7 June 2018)

Breakup dynamics of $C_2H_2^{3+} \rightarrow H^+ + H^+ + C_2^+$ induced by 50-keV/u Ne^{8+} ion impact is investigated employing a reaction microscope. All three ionic fragments in the final state are detected in coincidence, and their momentum vectors as well as the kinetic energies are determined. The kinetic-energy correlation spectrum of the two protons displays very rich structures. Utilizing the Newton diagrams and the Dalitz plots, different dissociation mechanisms corresponding to these structures are identified. It was found that, besides the concerted and sequential breakup, fragmentation mechanisms associated with different vibration modes including molecular bending and asymmetric stretching also make significant contributions. We analyzed the correlation between different fragmentation mechanisms and the kinetic-energy release (KER) and found that the sequential process occurs with higher KER while, in contrast, the concerted process mainly contributes to the lower KER. This behavior is entirely opposite to the breakup of the CO_2 molecule.

DOI: 10.1103/PhysRevA.97.062701

I. INTRODUCTION

The investigation of the fragmentation dynamics of multicharged polyatomic molecules is of fundamental interest in physics and chemistry and of great importance in numerous application fields such as plasma physics, chemistry of planetary atmospheres, and radiation damage of living tissues. The multiply ionized molecules can be produced efficiently by collision with ions, electrons, x-rays, or intense laser fields. These multicharged ions are unstable and readily break up due to the strong Coulomb repulsion between different ionic cores. With the help of the well-developed imaging techniques [1,2], it is now possible to detect all the fragmented cations in multicoincidence [3] and visualize the fragmentation dynamics in detail.

Three-body fragmentation of the polyatomic molecules has drawn great interest in recent years. This is due not only to the simplicity of a three-body process but also to the fundamental significance for understanding more complicated systems. Taking the heavily investigated CO_2 molecule as an example, Neumann *et al.* found that, besides the concerted fragmentation with two C=O chemical bonds breaking simultaneously, the sequential fragmentation with two bonds breaking one after the other also exists in the breakup of CO_2^{3+} [4]. They also found that the energy deposited into the parent ion plays a key role in switching between different pathways. The sequential process readily occurs with small energy deposition, while in contrast, the concerted process is preferred when more energies are deposited to the system. The existence of a sequential fragmentation process in the breakup of CO_2 was confirmed by following works [5–10]. Until now, the sequential and concerted fragmentation pathways have been identified for a variety of molecules, including the symmetric triatomic molecules CS_2 [11,12] and H_2O [13], the asymmetric triatomic molecules N_2O [14,15] and OCS [16], the organic molecules CH_4 [17] and C_6D_6 [18], and even in case of the van der Waals clusters N_2Ar, O_2Ar, O_2Xe [19], COAr [20], and $(CO)_2$ [21]. Until now, the sequential and concerted processes have mainly been discussed in the breakup of triatomic molecules. Few experimental works extended the consideration of the sequential and concerted fragmentation processes to polyatomic molecules consisting of more than three nuclei [17,18].

Acetylene (C_2H_2) is one of the smallest organic molecules in nature. It has been chosen as the prototype system for investigation of basic physical and chemical problems such as the cleavage of the C–H and C–C chemical bonds, and the acetylene-vinylidene isomerization. The fragmentation dynamics of C_2H_2 has been investigated by photoionization [22,23], electron collision [24–26], and ion collision [27–31]. Most of the existing experiments focus on the two-body fragmentation process [24,26,28,29,31], or detect only two fragments of a multibody breakup process [24–28,30,31]. Besides, the fragmentation processes of the trication $C_2H_2^{3+}$ have also been used to visualize the isomerization occurring on the cation or dication intermediate state in pump-probe measurements [32–35]. However, the experiments which detect all fragments in the final state in coincidence and focus on the three-body fragmentation dynamics of the trication $C_2H_2^{3+}$ are scarce. De *et al.* studied the fragmentation of $C_2H_2^{3+}$ in collision with Ar^{8+} and identified the bent structure of the $C_2H_2^{3+}$ trication by experimentally determining the $H^+ - C_2^+ - H^+$ angle. Such molecular bending was also observed in the x-ray-induced core-excited state of C_2H_2 [23]. The detailed investigation of the three-body fragmentation dynamics of $C_2H_2^{3+}$ is still absent.

*xushenyue@xjtu.edu.cn

†x.ma@impcas.ac.cn

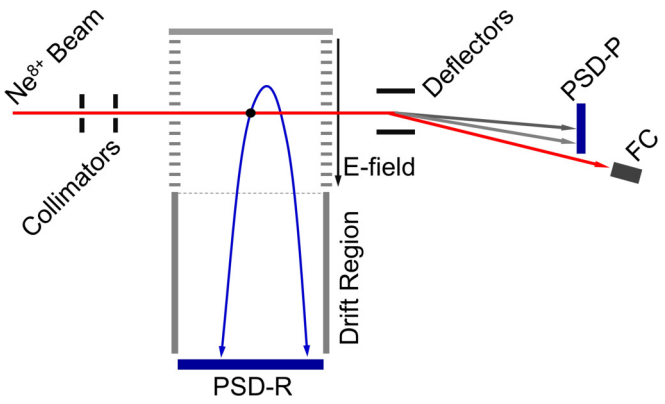

FIG. 1. Schematic diagram of experimental apparatus.

In the present work, we investigate the three-body fragmentation of C_2H_2 by highly charged ion collisions. We chose the Ne^{8+} ion as the projectile to produce the $C_2H_2{}^{3+}$ trication. The high-charge nature of Ne^{8+} makes it easy to remove more than one electron from the target. In our experiment, the velocity of the projectile is chosen as 1.4 atomic units (50 keV/u). It passes through the target in a timescale of 100 as, which is much faster than the nuclei motion. Consequently, vertical transitions between the neutral C_2H_2 and the $C_2H_2{}^{3+}$ ion occur during collision, and the parent $C_2H_2{}^{3+}$ ions are mainly lying in the ground or low-lying electronically excited states without deformation of the molecular geometry.

Among various fragmentation channels we focus on the three-body breakup channel

$$C_2H_2{}^{3+} \rightarrow H^+ + H^+ + C_2{}^+. \quad (1)$$

By detecting all the three fragments in coincidence, the momentum vector as well as the kinetic energy (KE) of each charged fragment is determined. The experimental data are displayed in the KE correlation spectrum of two protons, the Newton diagrams, and the Dalitz plots. Different fragmentation mechanisms are identified and discussed in detail.

II. EXPERIMENTS AND DATA ANALYSIS

The experiment was carried out with a reaction microscope [2] (also called cold target recoil-ion-momentum spectroscopy, COLTRIMS [1]) mounted on the 320 kV platform for multidisciplinary research with highly charged ions at the Institute of Modern Physics, Chinese Academy of Sciences. A schematic view of the experiment setup is shown in Fig. 1. Since details of the setup have been described elsewhere [36], only a brief introduction will be given here. The collimated 50-keV/u Ne^{8+} beam crosses the acetylene jet produced by the supersonic expansion of the pure acetylene gas with a stagnation pressure of 1.0 bar. The typical target density is estimated to be 5×10^{17} molecules/m^3. After collision, the ionic fragments are extracted toward the time and position sensitive detector for recoil ions (PSD-R in Fig. 1) by a uniform electric field of 180 V/cm. The electric field is perpendicular to both the projectile beam and the gas jet. The charge-changed projectiles are separated from the primary beam by an electrostatic deflector, and detected by another time and position sensitive detector (PSD-P in Fig. 1). A Faraday cup (FC) is used to collect the residual Ne^{8+} ions. The ionic fragments and the scattered Ne^{7+} (or Ne^{6+}) ions are measured in multicoincidence and stored in event-by-event mode.

During offline data analysis, the following two reactions which contribute to the $H^+ + H^+ + C_2{}^+$ fragmentation are considered:

$$Ne^{8+} + C_2H_2 \rightarrow Ne^{7+} + H^+ + H^+ + C_2{}^+ + 2e^-, \quad (2)$$

$$Ne^{8+} + C_2H_2 \rightarrow Ne^{6+} + H^+ + H^+ + C_2{}^+ + e^-. \quad (3)$$

The relative contributions of reactions (2) and (3) are 8.7 :1.

The momentum vector of each fragment is reconstructed according to the recorded time and position information, and consequently the kinetic energies of these particles are obtained. The overall momentum resolution for the $H^+ + H^+ + C_2{}^+$ channel is determined to be 8, 9, and 12 a.u. in the directions along the electric field, the projectile beam, and the gas jet, respectively.

The Newton diagrams and the Dalitz plots [37] are utilized to reveal details of the fragmentation dynamics. In our definition of the Newton diagram, the momentum vector of the proton with higher energy (denoted as H_a) is represented by an arrow along the horizontal axis fixed to 1.0 arbitrary unit. The momentum vectors of the other protons with lower energy (denoted as H_b) and of the $C_2{}^+$ are normalized to the momentum vector of H_a and displayed in the upper and lower half of the plot, respectively.

In our definition of the Dalitz plot, the coordinates X and Y are given by

$$X = \frac{P_{H_0}{}^2 - P_{H_1}{}^2}{\sqrt{3}\sum P_i^2}, \quad (4)$$

$$Y = \frac{P_{C_2}{}^2}{\sum P_i^2} - \frac{1}{3}, \quad (5)$$

where P_i with $i = 0, 1, 2$ represents the momentum of the two protons $H_0{}^+$, $H_1{}^+$, and the $C_2{}^+$ ions, respectively. We emphasize that, unlike the definition of the Newton diagram, the two protons are not distinguished according to their KE in our definition of the Dalitz plot. $H_0{}^+$ and $H_1{}^+$ here denote the first and the second of the two successively detected protons, respectively.

III. RESULTS AND DISCUSSION

A. Kinetic-energy correlation spectrum

For the channel $H^+ + H^+ + C_2{}^+$ studied here, the two protons take most of the kinetic-energy release (KER, defined as the sum energy of the three fragments in the final state) since the mass of a proton is only 1/12 that of the carbon nuclei. The KE distributions of these two protons could be very sensitive to the breakup mechanisms. We present the KE correlation spectrum of the two protons in Fig. 2. This figure displays a symmetric distribution with respect to the diagonal denoted as the gray dashed line. The rich structures shown here indicate that different fragmentation mechanisms may occur. For convenience, we label these structures A, B, and C in Fig. 2. From the KE correlation spectrum only we may

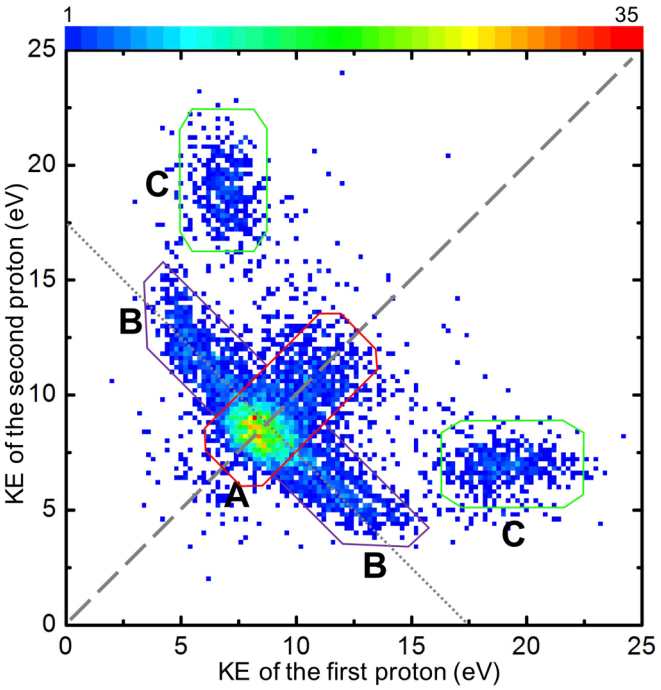

FIG. 2. KE correlation between the two protons. Events located in the different regions marked A, B, and C correspond to different fragmentation mechanisms. A: concerted fragmentation, B: asymmetric stretching, and C: sequential fragmentation. Gray dashed line is $y = x$ with the two protons taking the same KE, gray dotted line is $x + y = 17.5$ corresponding to the sum KE of 17.5 eV.

speculate that the region A with symmetric energy sharing between the two protons arises from the concerted cleavage of the two C–H bonds with the same length, while the winglike structure B and the isolated land C for which the KER is shared unequally between the two protons may originate from either an asymmetric geometry or the sequential breakup with the two protons emitted one after the other.

B. Momentum correlation spectra

To visualize the correlation between the three fragments and discriminate the fragmentation mechanisms in detail, we present the Newton diagrams and the Dalitz plots in Fig. 3. Figs. 3(a) and 3(b) present the Newton diagram and the Dalitz plot with all the measured data.

The correlation between the calculated momentum vectors of the three fragments is shown in Fig. 3(c). In this figure, the momentum correlation is only displayed for the areas covered by experimental data. Figures 3(d)–3(f) display the Newton diagrams and Figs. 3(g)–3(i) display the Dalitz plots with different KE filters A, B, and C, respectively. These KE filters determine the accessible areas in both the Dalitz plots and the Newton diagrams. The symmetric energy sharing between the two protons in region A restricts the experimental data to distribute only along $X = 0$ in the Dalitz plot. In contrast, the asymmetric energy sharing in both regions B and C determines that $X = 0$ is unaccessible in the Dalitz plots, and the momentum of C_2^+ shown in the Newton Diagrams should not be zero due to momentum balance between the three fragments.

The Newton diagram and the Dalitz plot for region A are shown in Figs. 3(d) and 3(g), respectively. We see an intense area around the point $(0, -1/3)$ in Fig. 3(g), which indicates that the concerted fragmentation with symmetric linear geometry is the major contribution of region A. The Newton diagram shown in Fig. 3(d) presents a scenario that the two protons are emitted back-to-back while leaving the C_2^+ ion almost at rest, which is also the signature of concerted fragmentation originating from the symmetric linear geometry. Nevertheless, we also see in Fig. 3(g) that the distribution extends from $Y = -1/3$ to around $Y = -0.1$, indicating that molecular bending also contributes to region A. The contribution of molecular bending is confirmed by the tail structure extending from the most intense area in the Newton diagram shown in Fig. 3(d).

In region B of Fig. 2 we see a strong KE correlation; when the KE of one proton decreases, the KE of the other proton increases. This is evidence that region B originates from asymmetric stretching since, for asymmetric stretching, the elongation of one C–H bond is always accompanied by the shortening of the other one. During the fragmentation process, the two C–H bonds break simultaneously; however, with different bond lengths. Consequently in such a process the C_2^+ ion obtains a reasonable amount of momentum due to the asymmetric repulsion from the two protons. This is consistent with the Newton diagram shown in Fig. 3(e), in which the most intense region appears at around $x = -0.4$ with the C_2^+ ion taking an amount of momentum. The Dalitz plot for region B is presented in Fig. 3(h). The major structure in this plot is marked by two black ovals. As can be seen in Fig. 3(c), in these two ovals the two protons are emitted back to back with different magnitude of the momentum vectors. Such a momentum correlation pattern confirms our conclusion that the major contribution for region B is the asymmetric stretching.

A weak /\-shaped structure marked D appears in Fig. 3(h). The /\-shaped structure is also observed in the Dalitz plot of region C, which is shown in Fig. 3(i) and marked E. We see in Fig. 3(c) that the mutual angle θ_{12} between the two protons changes gradually from 180° to around 60° along the gray dotted lines. We attribute such an evolution of the θ_{12} angle to the two-step sequential process, i.e.,

$$C_2H_2^{3+} \rightarrow H_a^+ + C_2H^{2+} \text{ (step 1)}, \quad (6)$$

$$C_2H^{2+} \rightarrow H_b^+ + C_2^+ \text{ (step 2)}, \quad (7)$$

and the rotation of the C_2H^{2+} ion occurs between the two steps. For the sequential process, there should be no obvious correlation between the KEs of the two protons since the emission of H_a is independent of step 2. Indeed, the KE distribution in region C of Fig. 2 shows that the KE of one proton does not change obviously as the KE of the other proton varies. In addition, Fig. 3(f) shows that the momenta of the proton and the C_2^+ are located on the semicircles marked by the dotted lines. This circular feature is another proof of the two-step fragmentation mechanism.

The above two-step analysis is also supported by our estimation of the timescale of step 1 and the rotational period of the intermediate C_2H^{2+} ion. We calculated the KEs of the two fragments in step 1 as the function of propagation time

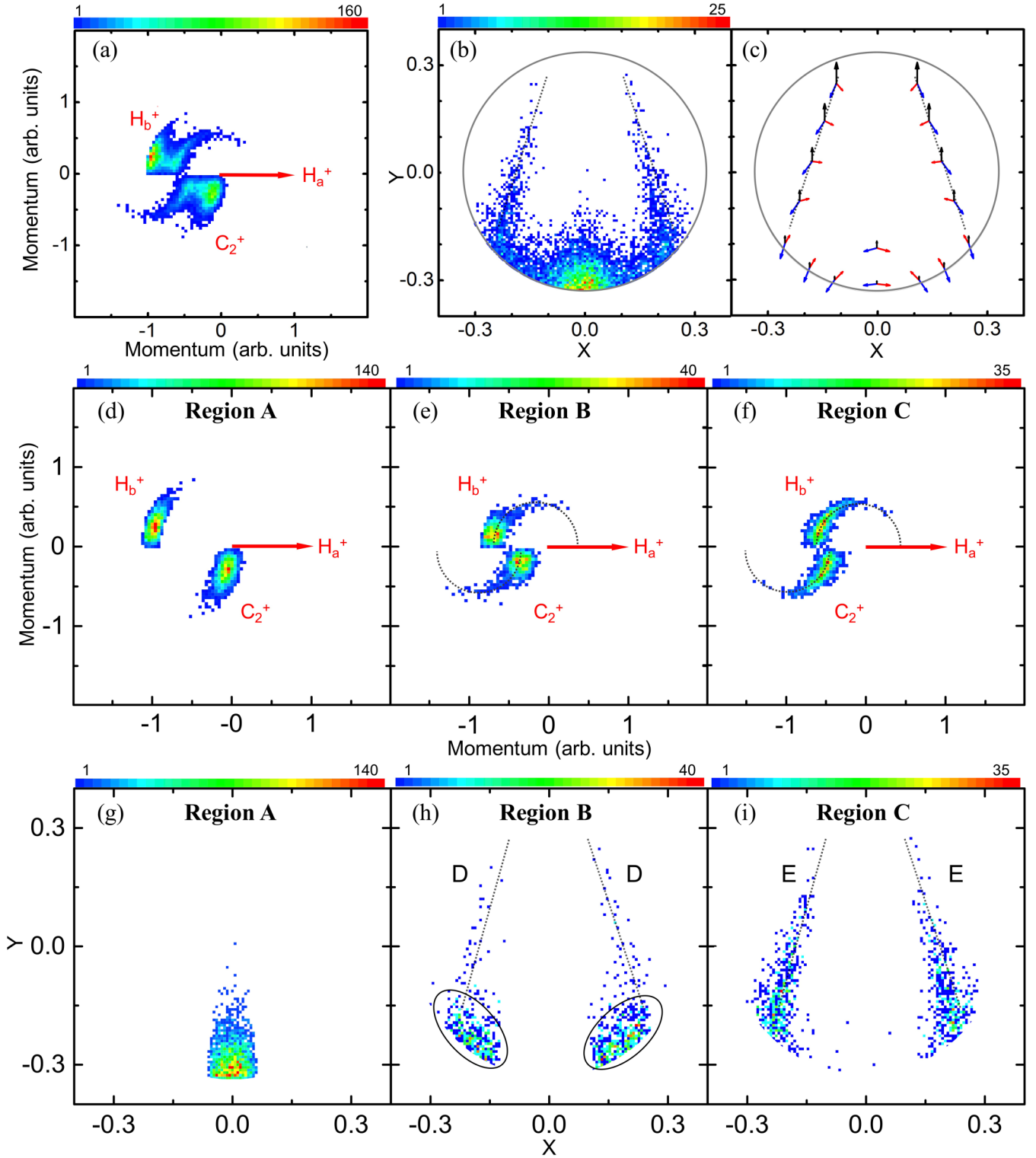

FIG. 3. (a) Newton diagram and (b) Dalitz plot with all the experimental data without KE filter. (c) Calculated momentum correlation between the three particles as the function of Dalitz coordinates (X,Y). The black, blue, and red arrows denote the momentum vectors of the C_2^+ ion, and the two protons H_1 and H_2, respectively. (d)–(f) Newton diagrams and (g)–(i) Dalitz plots with different KE filters A, B, and C shown in Fig. 2, respectively. The gray dotted lines in Figs. 3(b), 3(c), 3(h), and 3(i) are meant to guide the eye. They are locate at the same X and Y coordinates in each figure.

by assuming the C_2H^{2+} ion to be a point particle with charge and mass locating in the center of mass. The result shows that most of the Coulomb potential energy (∼80%) is converted to the KE in less than 10 fs. During proton emission, the C_2H^{2+} ion acquires an amount of angular momentum and rotates. For sequential breakup of CO_2, the half-rotational

period of the intermediate CO^{2+} is estimated to be around 89 fs [4]. One may expect that the half-rotational period for C_2H^{2+} in our case is even longer than this value since the measured momentum of the primary proton (about 50 a.u.) is smaller than the momentum of O^+ (about 150 a.u.) [4]. It is obvious that the timescale for emission of the proton in step 1 is much shorter than the half-rotational period of the intermediate C_2H^{2+} ion. We also see in Fig. 3(f) that the experimental data only covers part of the semicircles. This may indicate that the intermediate C_2H^{2+} ion only survives with a time shorter than its half-rotational period. Namely, the C_2H^{2+} ion fragments to a proton and a C_2^+ ion before rotating for a semicycle.

The weak /\-shaped structure marked D in Fig. 3(h) displays similar distributions as E in the Dalitz plot. The corresponding Newton diagram in Fig. 3(e) also displays semicircle structures which is similar to that in Fig. 3(f). We thus attribute D to another sequential fragmentation pathway. It can be seen in Fig. 2 that the KEs of the emitted protons for the events in region D are lower than region E. This difference may arise from different responsible electronic states of both the parent $C_2H_2^{3+}$ ion and the intermediate C_2H^{2+} ion. Different contributions to the sequential fragmentation were also identified for the CO_2 molecule. The relation between these different sequential pathways and the responsible electronic states were discussed in detail for CO_2 in Refs. [7,9].

C. Correlation between fragmentation mechanisms and kinetic-energy release

The C_2^+ ion, due to its high mass compared with the protons, makes only a negligible contribution to the overall KER. Therefore, the KER could be approximated by the sum of the KE of the two protons. This KER reflects the onset energy deposited into the target during collision. As is shown in Fig. 2, the main contribution for concerted fragmentation (region A) locates at a KER around 16.5 eV which probably arises from the ground electronic state of the parent $C_2H_2^{3+}$ ion. Besides, in region A we also see a broad distribution extending to KER around 23 eV along the diagonal (gray dashed) line, indicating that the excited electronic states may also contribute to the concerted process. It could also be seen in Fig. 2 that the KER of the fragmentation accompanied with asymmetric stretching (region B) are around 17.5 eV, which is probably also arising from the ground electronic state of $C_2H_2^{3+}$. In contrast, the two-step sequential fragmentation process (region C) results to higher KER around 25 eV.

For the fragmentation of the CO_2 molecule, many existing experiments have demonstrated that the sequential process mainly contributes to the lower part of the KER distribution. With the increasing of the KER, the sequential process becomes negligible and the concerted process makes the major contribution [4,7–9]. However, our results present a completely opposite behavior for the fragmentation of the C_2H_2 molecule. The sequential process is the dominant contribution to the 25 eV peak with the highest KER, while in contrast the concerted process contributes to the low KER.

The surviving time of the intermediate C_2H^{2+} ion populated to the metastable intermediate state is the key factor that determines whether the parent ion fragments sequentially or simultaneously. Our results indicate that the C_2H^{2+} ions related to the 16.5 eV peak in the KER curve are unstable and break immediately after its formation. In contrast, the C_2H^{2+} ions corresponding to the 25 eV peaks could survive long enough for rotation to occur before breakup. Nevertheless, the intermediate C_2H^{2+} ions could probably survive for a shorter time than half of their rotational period since the experimental data only covers part of the semicircle in the Newton diagram shown in Fig. 3(f).

IV. CONCLUSIONS

The $H^+ + H^+ + C_2^+$ fragmentation of $C_2H_2^{3+}$ is experimentally investigated by Ne^{8+} collisions. Utilizing the reaction microscope technique, all three fragments are measured in coincidence and their momentum vectors as well as KE are obtained. By combined analysis of the KE correlation spectrum, the Newton diagrams, and the Dalitz plots, different fragmentation mechanisms are clearly separated, and their relation to the vibrational modes are revealed. We found that, in addition to the direct concerted breakup of C_2H_2 in the vibrational ground state, vibrational excited states such as the molecular bending and the asymmetric stretching also contribute significantly. In addition, the sequential fragmentation process with the two protons emitted one after the other is also identified in the present study. We analyzed the correlation between different fragmentation mechanisms and the KER and observed a completely reversed trend with respect to that of the CO_2 molecule. For C_2H_2 the sequential process occurs with high KER and disappears when KER is low. Detailed information of the responsible electronic states and their potential-energy surfaces would be helpful for a deeper understanding of the fragmentation mechanisms.

ACKNOWLEDGMENTS

This work is supported by the National Key Research and Development Program of China under Grant No. 2017YFA0402300, and by the National Natural Science Foundation of China under Grants No. U1432122, No. 11674332, and No. U1532129. S.X. thanks Xueguang Ren and Enliang Wang for useful discussions. The authors acknowledge the staff of the 320 kV platform at Institute of Modern Physics, Chinese Academy of Sciences for their technical support.

[1] R. Dörner, V. Mergel, O. Jagutzki, L. Spielberger, J. Ullrich, R. Moshammer, and H. Schmidt-Böcking, Phys. Rep. **330**, 95 (2000).

[2] J. Ullrich, R. Moshammer, A. Dorn, R. Dörner, L. Ph. H. Schmidt, and H. Schmidt-Böcking, Rep. Prog. Phys. **66**, 1463 (2003).

[3] M. Pitzer, M. Kunitski, A. S. Johnson, T. Jahnke, H. Sann, F. Sturm, L. Ph. H. Schmidt, H. Schmidt-Böcking, R. Dörner, J. Stohner, J. Kiedrowski, M. Reggelin, S. Marquardt, A. Schießer, R. Berger, and M. S. Schöffler, Science **341**, 1096 (2013).

[4] N. Neumann, D. Hant, L. Ph. H. Schmidt, J. Titze, T. Jahnke, A. Czasch, M. S. Schöffler, K. Kreidi, O. Jagutzki, H.

Schmidt-Böcking, and R. Dörner, Phys. Rev. Lett. **104**, 103201 (2010).
[5] C. Wu, C. Wu, D. Song, H. Su, Y. Yang, Z. Wu, X. Liu, H. Liu, M. Li, Y. Deng, Y. Liu, L. Y. Peng, H. Jiang, and Q. Gong, Phys. Rev. Lett. **110**, 103601 (2013).
[6] X. Wang, Y. Zhang, D. Lu, G. C. Lu, B. Wei, B. H. Zhang, Y. J. Tang, R. Hutton, and Y. Zou, Phys. Rev. A **90**, 062705 (2014).
[7] E. Wang, X. Shan, Z. Shen, M. Gong, Y. Tang, Y. Pan, K.-C. Lau, and X. Chen, Phys. Rev. A **91**, 052711 (2015).
[8] A. Khan, L. C. Tribedi, and D. Misra, Phys. Rev. A **92**, 030701 (2015).
[9] S. Yan, X. L. Zhu, P. Zhang, X. Ma, W. T. Feng, Y. Gao, S. Xu, Q. S. Zhao, S. F. Zhang, D. L. Guo, D. M. Zhao, R. T. Zhang, Z. K. Huang, H. B. Wang, and X. J. Zhang, Phys. Rev. A **94**, 032708 (2016).
[10] J. Rajput, T. Severt, B. Berry, B. Jochim, P. Feizollah, B. Kaderiya, M. Zohrabi, U. Ablikim, F. Ziaee, K. Raju P., D. Rolles, A. Rudenko, K. D. Carnes, B. D. Esry, and I. Ben-Itzhak, Phys. Rev. Lett. **120**, 103001 (2018).
[11] A. Hishikawa, H. Hasegawa, and K. Yamanouchi, Chem. Phys. Lett. **361**, 245 (2002).
[12] R. Guillemin, P. Decleva, M. Stener, C. Bomme, T. Marin, L. Journel, T. Marchenko, R. K. Kushawaha, K. Jänkälä, N. Trcera, K. P. Bowen, D. W. Lindle, M. N. Piancastelli, and M. Simon, Nat. Commun. **6**, 6166 (2015).
[13] R. Singh, P. Bhatt, N. Yadav, and R. Shanker, J. Phys. B: At. Mol. Opt. Phys. **46**, 085203 (2013).
[14] P. Bhatt, R. Singh, N. Yadav, and R. Shanker, Phys. Rev. A **86**, 052708 (2012).
[15] A. Khan, L. C. Tribedi, and D. Misra, Phys. Rev. A **96**, 012703 (2017).
[16] Z. Shen, E. Wang, M. Gong, X. Shan, and X. Chen, J. Chem. Phys. **145**, 234303 (2016).
[17] Y. Zhang, T. Jiang, L. Wei, D. Luo, X. Wang, W. Yu, R. Hutton, Y. Zou, and B. Wei, Phys. Rev. A **97**, 022703 (2018).
[18] A. Matsuda, M. Fushitani, R. D. Thomas, V. Zhaunerchyk, and A. Hishikawa, J. Phys. Chem. A **113**, 2254 (2009).
[19] J. Wu, M. Kunitski, L. Ph. H. Schmidt, T. Jahnke, and R. Dörner, J. Chem. Phys. **137**, 104308 (2012).
[20] X. Gong, M. Kunitski, L. P. H. Schmidt, T. Jahnke, A. Czasch, R. Dörner, and J. Wu, Phys. Rev. A **88**, 013422 (2013).
[21] X. Ding, M. Haertelt, S. Schlauderer, M. S. Schuurman, A. Yu. Naumov, D. M. Villeneuve, A. R. W. McKellar, P. B. Corkum, and A. Staudte, Phys. Rev. Lett. **118**, 153001 (2017).
[22] T. Kinugawa, P. Lablanquie, F. Penent, J. Palaudoux, and J. H. D. Eland, J. Electron Spectrosc. Relat. Phenom. **141**, 143 (2004).
[23] N. Saito, M. Nagoshi, M. Machida, I. Koyano, A. De Fanis, and K. Ueda, Chem. Phys. Lett. **393**, 295 (2004).
[24] S. J. King and S. D. Price, J. Chem. Phys. **127**, 174307 (2007).
[25] R. Flammini, M. Satta, E. Fainelli, and L. Avaldi, Phys. Rev. A **83**, 014501 (2011).
[26] R. Flammini, M. Satta, E. Fainellia, and L. Avaldia, Phys. Chem. Chem. Phys. **13**, 19607 (2011).
[27] S. De, J. Rajput, A. Roy, P. N. Ghosh, and C. P. Safvan, J. Chem. Phys. **127**, 051101 (2007).
[28] S. De, J. Rajput, A. Roy, P. N. Ghosh, and C. P. Safvan, Phys. Rev. A **77**, 022708 (2008).
[29] M. A. Parkes, J. F. Lockyear, and S. D. Price, Int. J. Mass Spectrom. **280**, 85 (2009).
[30] T. Mizuno, T. Yamada, H. Tsuchida, Y. Nakai, and A. Itoh, J. Phys.: Conf. Ser. **163**, 012039 (2009).
[31] S. Yoshida, T. Majima, T. Asai, M. Matsubara, H. Tsuchida, M. Saito, and A. Itoh, Nucl. Instrum. Methods Phys. Res., Sect. B **408**, 203 (2017).
[32] A. Hishikawa, A. Matsuda, M. Fushitani, and E. J. Takahashi, Phys. Rev. Lett. **99**, 258302 (2007).
[33] A. Hishikawa, A. Matsuda, E. J. Takahashi, and M. Fushitani, J. Chem. Phys. **128**, 084302 (2008).
[34] H. Ibrahim, B. Wales, S. Beaulieu, B. E. Schmidt, N. Thiré, E. P. Fowe, É. Bisson, C. T. Hebeisen, V. Wanie, M. Giguére, J.-C. Kieffer, M. Spanner, A. D. Bandrauk, J. Sanderson, M. S. Schuurman, and F. Légaré, Nat. Commun. **5**, 4422 (2014).
[35] C. Burger, N. G. Kling, R. Siemering, A. S. Alnaser, B. Bergues, A. M. Azzeer, R. Moshammer, R. de Vivie-Riedle, M. Kübel, and M. F. Klingab, Faraday Discuss. **194**, 495 (2016).
[36] X. Ma, R. T. Zhang, S. F. Zhang, X. L. Zhu, W. T. Feng, D. L. Guo, B. Li, H. P. Liu, C. Y. Li, J. G. Wang, S. C. Yan, P. J. Zhang, and Q. Wang, Phys. Rev. A **83**, 052707 (2011).
[37] R. H. Dalitz, Philos. Mag. **44**, 1068 (1953).